

A mechanical model of vehicle-slab track coupled system with differential subgrade settlement

Yu Guo^a, Wanming Zhai* and Yu Sun^b

Train and Track Research Institute, State Key Laboratory of Traction Power, Southwest Jiaotong University, No. 111,
First Section, North of Second Ring Road, Chengdu, People's Republic of China

(Received April 12, 2017, Revised September 25, 2017, Accepted January 23, 2018)

Abstract. Post-construction subgrade settlement especially differential settlement, has become a key issue in construction and operation of non-ballasted track on high-speed railway soil subgrade, which may also affect the dynamic performance of passing trains. To estimate the effect of differential subgrade settlement on the mechanical behaviors of the vehicle-slab track system, a detailed model considering nonlinear subgrade support and initial track state due to track self-weight is developed. Accordingly, analysis aiming at a typical high-speed vehicle coupled with a deteriorated slab track owing to differential subgrade settlement is carried out, in terms of two aspects: (i) determination of an initial mapping relationship between subgrade settlement and track deflections as well as contact state between track and subgrade based on a semi-analytical method; (ii) simulation of dynamic performance of the coupled system by employing a time integration approach. The investigation indicates that subgrade settlement results in additional track irregularity, and locally, the contact between the concrete track and the soil subgrade is prone to failure. Moreover, wheel-rail interaction is significantly exacerbated by the track degradation and abnormal responses occur as a result of the unsupported areas. Distributions of interlaminar contact forces in track system vary dramatically due to the combined effect of track deterioration and dynamic load. These may not only intensify the dynamic responses of the coupled system, but also have impacts on the long-term behavior of the track components.

Keywords: slab track; subgrade settlement; vehicle-track coupled dynamics; track deflections; contact failure

1. Introduction

In the last decade, there has been a substantial boom in the development and construction of high-speed railway in China. The advantages of superior integrity and stability make the non-ballasted track the preferred track type. The increasing demands for higher speed and traffic volume as well as concerns over the running safety, ride comfort and lower track lifecycle cost have resulted in fresh challenges need to be addressed. A major issue is to build non-ballasted tracks on soil subgrades in view of the post-construction settlement. Soft soil ground with large compressibility and low permeability is widely distributed in China, which is settlement-prone in railway construction (Wang *et al.* 2015). Differential settlement on soft soil subgrade along the high-speed railway lines commonly appears due to the non-uniform soil property, variation of groundwater-level and other defects of subgrade (Chen *et al.* 2014, Olivier *et al.* 2016). Relevant monitoring-data (Li *et al.* 2007, Zeng *et al.* 2009) have shown that, in some regions, subgrade settlements of high-speed railways are quite serious, and even sharply change the original gradient of the railway line

and result in speed restriction.

In the presence of differential subgrade settlement, track structures settle along with infrastructure as a consequence of track self-weight and dynamic load. Track geometry is thus degraded, turning into additional track irregularities, which eventually intensifies the wheel-rail interaction (Dahlberg 2003, Kouroussis *et al.* 2015a). Moreover, in view of the characteristic of integrality and the limited adjustment of the non-ballasted track, concrete track is suspected to be separated from the soil subgrade locally, inducing 'hanging' phenomenon, where the subgrade support is discontinuous. When trains pass through, these unsupported areas are slapped periodically, implying that the contact between track and subgrade in these local areas may be lost and/or re-established during dynamic loads (Varandas *et al.* 2011). With the increasing train speed and load, the settlement-induced track irregularities and the unevenly distributed track support will accelerate the deterioration of track components, and in turn induce abnormal dynamic responses to the vehicle-track system. However, issues related to track defects due to the poor geotechnical performance of the earthworks can be difficult to detect and complex to solve because the infrastructure is generally inaccessible. Maintenance and repair works on the infrastructure normally imply longer and costly restrictions to train operation than the regular maintenance works on the track (Paixão *et al.* 2015).

Most of the previous studies on track settlement focused on the accumulated track deterioration due to cyclic traffic load, where the settlement was basically predicted by

*Corresponding author, Ph.D.

E-mail: wmzhai@home.swjtu.edu.cn

^aPh.D. Student

E-mail: guoyu20081586@163.com

^bPh.D. Student

E-mail: sunyu.9003@163.com

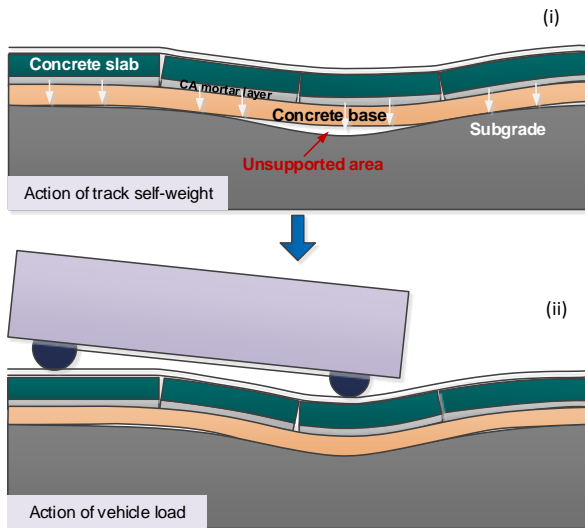


Fig. 1 Schematic diagram of the method

empirical models as listed in Ref. (Li *et al.* 2014). Few works placed emphasis on the transmission of the existing differential settlement from the infrastructure to the upper track structure. It has been pointed out by Varandas *et al.* (2014) that an abrupt change of track stiffness and differential settlement give rise to track degradation. Taking account of hanging sleepers, Zou *et al.* (2011) carried out a laboratory test to determine the mapping relationship between the differential ballast settlement and the rail deflection. Chen *et al.* (2015) also made effort to clarify the pier settlement-induced track irregularities of non-ballasted tracks in high-speed railways through an analytical approach.

As for the dynamic analysis of the vehicle-non-ballasted track system subjected to differential subgrade settlement, a number of investigations have been conducted, where the settlement profile was simulated as a function of settlement amplitude and wavelength. For instance, Han and Yao (2007) analyzed the settlement-induced dynamic characteristics based on a vehicle-track coupled model, which indicated that the differential settlement had a significant impact on the ride comfort of vehicles and aroused additional stresses on track structures. The results also related differential settlement limits to train speed. Although these works have gained some beneficial suggestions, there are still limitations. One of them is assuming that the differential subgrade settlement is entirely translated into rail irregularities, where the transmission and suppression of the differential settlement in track layers from bottom to top are neglected, as well as the non-uniform subgrade support. In some other studies, track weight and imperfect contact between track and subgrade were considered, e.g., Xu *et al.* (2012) developed a vehicle-track-subgrade model by describing the track on subgrade as a finite element model, and effects of differential subgrade settlement on dynamic performances of different types of non-ballasted tracks were compared. An investigation on developing appropriate standards for allowable differential subgrade settlement according to the dynamic responses of the vehicle-track system was

presented by Zhang *et al.* (2016). However, the settlement-induced initial track irregularities and the latent separations underneath the concrete track, and their influences on the dynamic behaviors of the system, have not been investigated in detail.

On this account, this paper presents a mechanical model to analyze the dynamic responses of the coupled vehicle-slab track system in the presence of differential subgrade settlement, taking the non-tension subgrade support and track self-weight into account. A semi-analytical method is included to detect the initial track state in terms of the locations of the initial unsupported areas and the settlement-induced track irregularities, which ultimately exert impact on dynamic performance of the vehicle-track system.

The rest of the paper is structured as follows: the analysis scheme is illustrated in Section 2. The mechanical model, which includes the semi-analytical approach to figure out the mapping relationship between subgrade settlement and track irregularities as well as the numerical integration of the vehicle-track coupled dynamics, are unfolded in Section 3. On this basis, a demonstration example according to the typical high-speed vehicle and slab track employed in China is presented in Section 4. Finally, relevant conclusions are drawn in Section 5.

2. Description of the analysis scheme

The proposed model is applied to investigate the effect of differential subgrade settlement on the mechanical behaviors of the vehicle-track system. As depicted in Fig. 1, the simulation procedure is mainly divided into two stages:

(i) Preliminarily, the effect of the vehicle passage is omitted. As a consequence of the differential subgrade settlement, the track structure gradually settles down to a steady position subjected to track self-weight. The static analysis based on a semi-analytical method is performed to obtain the settlement-induced track deflections and the eventual contact state between the track and the subgrade. In this stage, the initial track state before dynamic analysis is determined.

(ii) Lay the moving vehicle on the degraded track, dynamic responses of the vehicle-track coupled system can be obtained by means of a numerical integration method.

Fig. 2 shows the flowchart of the analysis scheme.

3. Characterization of the mechanical model

Previous studies indicate that the analysis of the vehicle-track coupled system in the presence of track/wheel imperfections generally utilize the vehicle-track coupled model with four essential components (Shabana *et al.* 2001, Zhu *et al.* 2010 and Kouroussis *et al.* 2015b): (i) a vehicle model; (ii) a track model; (iii) a wheel-rail contact model; and (iv) a track/wheel imperfection model. In this work, a 10-DOF (degrees of freedom) vehicle subsystem (i.e., seven vertical displacements and three pitch motions) and a three-layer track subsystem coupled through the Hertz nonlinear wheel-rail contact (Zhai *et al.* 2009) are employed to study

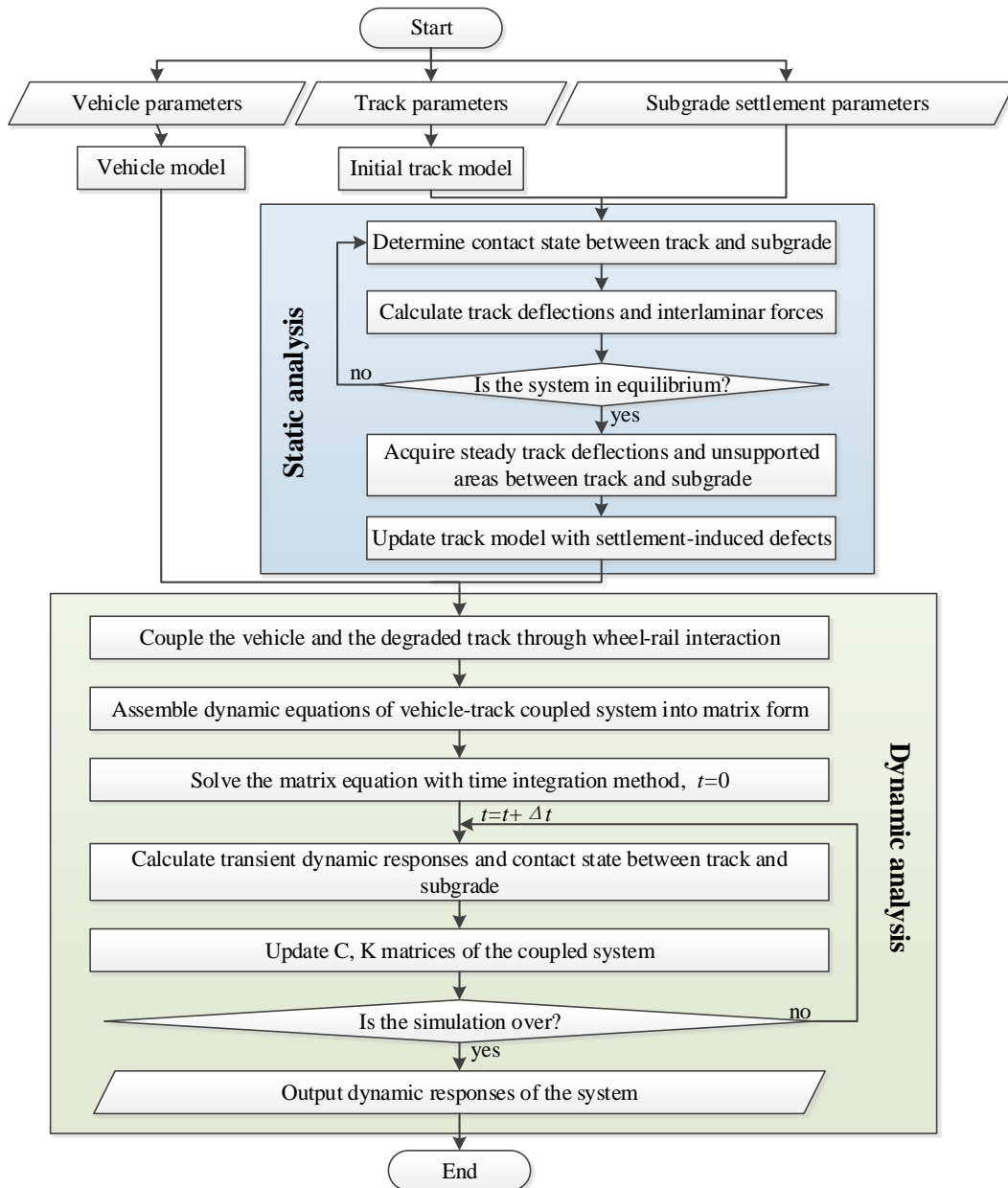


Fig. 2 Calculation flowchart of the scheme

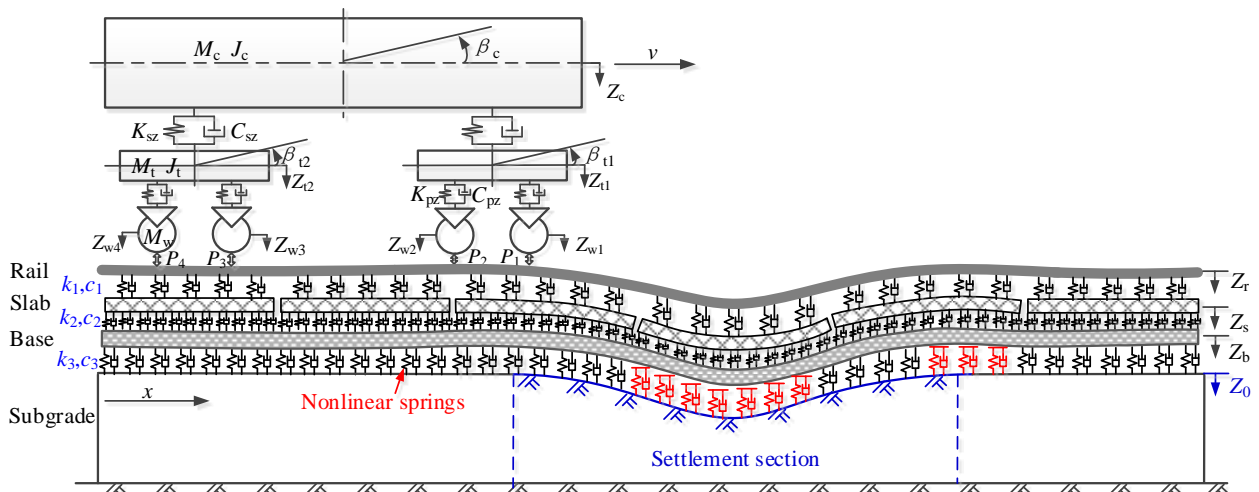


Fig. 3 Vehicle-slab track coupled model with differential subgrade settlement

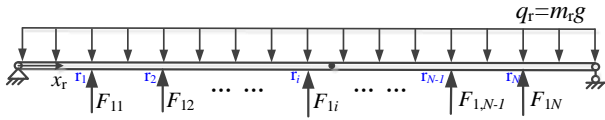


Fig. 4 Force diagram of rail

the dynamic responses of the system by taking the differential subgrade settlement into account, as shown in Fig. 3 for the side view.

The high-speed vehicle is modelled as a multi-rigid-body consists of a car body, two bogie frames and four wheelsets that are connected via the primary (K_{pz} , C_{pz}) and secondary (K_{sz} , C_{sz}) suspensions represented by spring-damping elements. The vertical and pitch motion for both car body (Z_c , β_c) and bogies (Z_b , β_b) together with the vertical motion of each wheel (Z_w) are investigated. In this case, the vehicle structure is considered to have 10 degrees of freedom.

The slab track, which is widely constructed in Chinese high-speed railways, is employed in the analysis. The slab track is composed of rail, fastener systems, concrete slabs, mortar layer and concrete base from the top down. Taking account of the subgrade settlement along the railway line, the non-ballasted track is built as multilayer composite beams on a non-tension Winkler foundation. In the model, the rail and the concrete base are modelled by the simply supported long beam, and the slabs are modelled by the free-free short beam without connection between adjacent slabs. Both the fastener systems and the mortar layer, the elasticity providers, are simulated as discrete spring-damping elements. In practice, the subgrade underneath the track does not provide any tensile resistance, thus, nonlinear springs are considered to account for the non-tension subgrade support. Existing differential settlement of subgrade represented by a certain stiffness pattern is regarded as nonlinear boundary conditions of the system.

Note that the above-presented model is a common model for both static analysis and dynamic analysis mentioned above. In the static analysis on initial track conditions considering the settlement-induced track level and unsupported areas, the vehicle part and the damping elements are omitted.

3.1 Semi-analytical solution for initial track state

3.1.1 Rail deflection

Taking track self-weight into consideration, the rail is subjected to the fastener forces and its own gravity at the steady state, as shown in Fig. 4.

For each rail node r_i ($i = 1 \sim N$, N is the number of fastener springs) at different fastener positions, the vertical deflection Z_{ri} can be expressed as

$$Z_{ri} = -\sum_{j=1}^N w_{ij}^{(1)} F_{1j} + u_i^{(1)} \cdot q_1 \quad (1)$$

where F_{1j} is the force of the j th fastener spring, q_1 is the gravity of the rail per unit length; $w_{ij}^{(1)}$ and $u_i^{(1)}$ are the corresponding displacements of node r_i respectively caused by the unit force acted on node r_j , and the unit uniform load

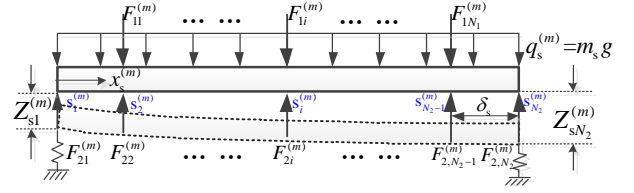


Fig. 5 Force diagram of slab

exerted on the beam. According to the deflection formula of the simply supported beam, $w_{ij}^{(1)}$ and $u_i^{(1)}$ can be calculated by

$$\begin{cases} w_{ij} = \begin{cases} \frac{b_j x_i}{6EI} (l^2 - x_i^2 - b_j^2), & \text{for } i \leq j \\ \frac{b_j}{6EI} \left[\frac{l}{b_j} (x_i - a_j)^3 + (l^2 - b_j^2) x_i - x_i^3 \right], & \text{for } i > j \end{cases} \\ u_i = \frac{x_i}{24EI} (l^3 - 2lx_i^2 + x_i^3) \end{cases} \quad (2)$$

where i and j denotes two nodes on the beam, x_i is the coordinate of the i th node, $a_j = x_j$, $b_j = l - x_j$. l and EI are the length and the flexural rigidity of the beam of the beam, respectively.

3.1.2 Slab deflection

Different from the rail beam, the beam for modelling the slab is free at two ends. Based on this assumption, the deflection of the free-free beam is considered as the superposition of: (i) the elastic deflection as a simply supported beam; (ii) the rigid displacement as an integral rigid body determined by the displacements at its two ends. Fig. 5 illustrates the forces and the deflection of the m th slab.

The numbers of the fastener spring nodes and the mortar spring nodes on one slab are notated as N_1 and N_2 respectively. For each node $s_i^{(m)}$ ($i = 2 \sim N_2 - 1$) on the m th slab, the vertical deflection $Z_{si}^{(m)}$ is calculated as

$$Z_{si}^{(m)} = \sum_{j=1}^{N_1} w_{ij}^{(2)} F_{1j}^{(m)} - \sum_{j=2}^{N_2-1} w_{ij}^{(2)} F_{2j}^{(m)} + u_i^{(2)} \cdot q_s^{(m)} + \bar{Z}_{si}^{(m)} \quad (3)$$

where $F_{2j}^{(m)}$ is the force of the j th mortar spring, $q_s^{(m)}$ is the gravity of the slab per unit length; $w_{ij}^{(2)}$ and $u_i^{(2)}$ are the corresponding displacements of node s_i respectively caused by the unit force acted on node s_j , and the unit uniform load exerted on the beam; $\bar{Z}_{si}^{(m)}$ is the rigid displacement caused by the mortar springs at two ends, which can be calculated as

$$\bar{Z}_{si}^{(m)} = Z_{s1}^{(m)} + \frac{Z_{sN_2}^{(m)} - Z_{s1}^{(m)}}{l_s} \cdot (i-1)\delta_s \quad (4)$$

where l_s is the length of slab, δ_s is the spacing between two adjacent mortar springs.

3.1.3 Concrete base deflection

Similar to the rail beam, the force diagram of the concrete base is shown in Fig. 6. As a simply supported beam, the vertical deflection Z_{bi} of each node b_i ($i = 1 \sim M$, M is the number of the subgrade springs) can be expressed as

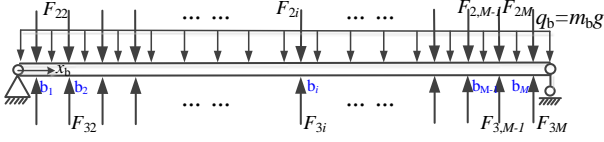


Fig. 6 Force diagram of concrete base

$$Z_{bi} = \sum_{j=1}^M w_{ij}^{(3)} F_{2j} - \sum_{j=1}^M w_{ij}^{(3)} F_{3j} + u_i^{(3)} \cdot q_b \quad (5)$$

where F_{3j} is the force of the j th subgrade spring, q_b is the gravity of the base per unit length. $w_{ij}^{(3)}$ and $u_i^{(3)}$ are the corresponding displacements of node b_i respectively caused by the unit force acted on node b_j , and the unit uniform load exerted on the beam.

3.1.4 Solving procedure

Forces of the fastener spring, the mortar layer spring and the subgrade spring at each node r_i , s_i and b_i are calculated by Eq. (6).

$$\begin{cases} F_{1i} = k_1(Z_{ri} - Z_{si}) \\ F_{2i} = k_2(Z_{si} - Z_{bi}) \\ F_{3i} = k_3 H_i(Z_{bi} - Z_{0i}) \end{cases} \quad (6)$$

where Z_{0i} is the initial displacement of subgrade settlement at each node; k_1 , k_2 and k_3 are stiffness of the fastener spring, mortar spring and subgrade spring, respectively. Since the non-tension subgrade spring is utilized, the step function H is employed to reflect the local contact state between the track and the subgrade. The value of H_i at each node can be described as

$$H_i = \begin{cases} 1, & \text{for } Z_{bi} > Z_{0i} \text{ (supported)} \\ 0, & \text{for } Z_{bi} \leq Z_{0i} \text{ (unsupported)} \end{cases} \quad (7)$$

Combine the above equations and assemble them in the matrix form as

$$\begin{bmatrix} \mathbf{E} + k_1 \mathbf{W}_1 & -k_1 \mathbf{W}_1 & \mathbf{0} \\ -k_1 \mathbf{W}_2 & \mathbf{E} + k_1 \mathbf{W}_2 + k_2 \mathbf{W}_2 & -k_2 \mathbf{W}_2 \\ \mathbf{0} & -k_2 \mathbf{W}_3 & \mathbf{E} + k_2 \mathbf{W}_3 + k_3 \mathbf{H} \cdot \mathbf{W}_3 \end{bmatrix} \begin{Bmatrix} \mathbf{Z}_r \\ \mathbf{Z}_s \\ \mathbf{Z}_b \end{Bmatrix} = \begin{Bmatrix} q_r \mathbf{U}_1 \\ q_s \mathbf{U}_2 \\ q_b \mathbf{U}_3 + k_3 \mathbf{H} \cdot \mathbf{W}_3 \cdot \mathbf{Z}_0 \end{Bmatrix} \quad (8)$$

where \mathbf{Z}_r , $\mathbf{Z}_s = \{\mathbf{Z}_s^{(1)}, \dots, \mathbf{Z}_s^{(m)}, \dots, \mathbf{Z}_s^{(N_s)}\}$ (N_s is the number of slabs) and \mathbf{Z}_b are the vector form of Z_{ri} , Z_{si} and Z_{bi} ; \mathbf{E} is the unit matrix; \mathbf{H} is a diagonal matrix comprised by H_i ; \mathbf{W}_1 , \mathbf{W}_2 , \mathbf{W}_3 and \mathbf{U}_1 , \mathbf{U}_2 , \mathbf{U}_3 are the matrix form of $w_{ij}^{(1)}$, $w_{ij}^{(2)}$, $w_{ij}^{(3)}$ and $u_i^{(1)}$, $u_i^{(2)}$, $u_i^{(3)}$.

To solve this nonlinear equation, the successive approximation method is adopted:

(i) Before the first iterative step, it is assumed that the concrete base of the non-ballasted track is completely in contact with the subgrade.

(ii) Then the track deflections calculated by Eq. (8) are extracted to determine the unsupported areas and the stiffness of the subgrade springs in the next step according

to Eq. (7).

(iii) Using the updated stiffness to re-calculate Eq. (8) and repeat procedure (ii) until convergence.

3.2 Numerical solution for vehicle-track coupled dynamics

3.2.1 Dynamic equations

By using the system of coordinates moving along the track with vehicle speed, the vibration equations of motions of the multi-rigid body system can be obtained according to the D'Alembert's principle. The dynamic equation of the vehicle system can be described in form of second order differential equations in the time domain.

$$\mathbf{M}_v \ddot{\mathbf{X}}_v + \mathbf{C}_v \dot{\mathbf{X}}_v + \mathbf{K}_v \mathbf{X}_v = \mathbf{P}_v \quad (9)$$

where \mathbf{M}_v , \mathbf{C}_v and \mathbf{K}_v are the mass, stiffness and damping matrices of the vehicle subsystem; \mathbf{X}_v , $\dot{\mathbf{X}}_v$ and $\ddot{\mathbf{X}}_v$ are the displacement, velocity and acceleration vectors of the vehicle subsystem; \mathbf{P}_v is the generalized force vector of the vehicle subsystem. The detailed explanations of this equation can be found in Zhai (2015).

Taking the track weight and the non-tension support of subgrade into consideration, the vibration equations of the rail, the m th slab and the concrete base can be written as

$$\begin{cases} E_r I_r \frac{\partial^4 Z_r(x, t)}{\partial x^4} + m_r \frac{\partial^2 Z_r(x, t)}{\partial t^2} = m_r g \\ - \sum_{i=1}^N F_{1i}(t) \delta(x - x_i) + \sum_{j=1}^4 P_j(t) \delta(x - x_{wj}) \\ E_s I_s \frac{\partial^4 Z_s^{(m)}(x, t)}{\partial x^4} + m_s \frac{\partial^2 Z_s^{(m)}(x, t)}{\partial t^2} = m_s g \\ + \sum_{i=1}^{N_1} F_{1i}^{(m)}(t) \delta(x^{(m)} - x_i^{(m)}) - \sum_{j=1}^{N_2} F_{2j}^{(m)}(t) \delta(x^{(m)} - x_j^{(m)}) \\ E_b I_b \frac{\partial^4 Z_b(x, t)}{\partial x^4} + m_b \frac{\partial^2 Z_b(x, t)}{\partial t^2} = m_b g \\ + \sum_{i=1}^{N_3 \times N_3} F_{2i}(t) \delta(x - x_i) - \sum_{j=1}^M F_{3j}(t) \delta(x - x_j) \end{cases} \quad (10)$$

where $Z_r(x, t)$, $Z_s^{(m)}(x, t)$ and $Z_b(x, t)$ are vibration displacement of the rail, the m th slab and the base at time t , $P_j(t)$ ($j = 1 \sim 4$) is the motion coordinate of the j th wheelset at time t ; forces of each fastener spring, mortar spring and subgrade spring $F_{1i}(t)$, $F_{2i}(t)$ and $F_{3i}(t)$ can be calculated by

$$\begin{cases} F_{1i}(t) = k_1 [Z_r(x_i, t) - Z_s(x_i, t)] \\ + c_1 [\dot{Z}_r(x_i, t) - \dot{Z}_s(x_i, t)] \\ F_{2i}^{(m)}(t) = k_2 [Z_r^{(m)}(x_i, t) - Z_s^{(m)}(x_i, t)] \\ + c_2 [\dot{Z}_r^{(m)}(x_i, t) - \dot{Z}_s^{(m)}(x_i, t)] \\ F_{3i}(t) = H_{di} \{ k_3 [Z_b(x_i, t) - Z_0(x_i)] + c_3 \dot{Z}_b(x_i, t) \} \end{cases} \quad (11)$$

where $\dot{Z}_r(x_i, t)$, $\dot{Z}_r^{(m)}(x_i, t)$, and $\dot{Z}_b(x_i, t)$ are the vibration velocity of the rail, the m th slab and the base respectively; $Z_0(x_i)$ is the differential subgrade settlement value; k_1 , k_2 , k_3 and c_1 , c_2 , c_3 are stiffness and damping

coefficient of the fastener spring, the mortar spring and subgrade spring respectively; H_{di} represents the transient contact between track and subgrade, which is similar to Eq. (7) as

$$H_{di} = \begin{cases} 1, & \text{for } Z_b(x_i, t) > Z_0(x_i) \text{ (supported)} \\ 0, & \text{for } Z_b(x_i, t) \leq Z_0(x_i) \text{ (unsupported)} \end{cases} \quad (12)$$

Based on Ritz method, Eq. (10) can be rewritten into the second order differential equations as follows

$$\begin{cases} \ddot{q}_{rk}(t) + \frac{E_r I_r}{m_r} \left(\frac{k\pi}{l} \right)^4 q_{rk}(t) = C_{rk} \\ - \sum_{i=1}^{N_r} F_{1i}(t) Y_{rk}(x_i) + \sum_{j=1}^4 p_j(t) Y_{rk}(x_{w_j}), & k = 1 \sim NM_r \\ m_s l \ddot{T}_k^{(m)}(t) + E_s I_s l_s \beta_k^4 T_k^{(m)}(t) = D_k \\ + \sum_{i=1}^{N_1} F_{1i}(t) X_k^{(m)}(x_i) - \sum_{j=1}^{N_2} F_{2j}(t) X_k^{(m)}(x_j), & k = 1 \sim NM_s \\ \ddot{q}_{bk}(t) + \frac{E_b I_b}{m_b} \left(\frac{k\pi}{l} \right)^4 q_{bk}(t) = C_{bk} \\ + \sum_{i=1}^{N_3 \times N_s} F_{2i}(t) Y_{bk}(x_i) - \sum_{j=1}^M F_{3j}(t) Y_{bk}(x_j), & k = 1 \sim NM_b \end{cases} \quad (13)$$

In Eq. (13), $q_{rk}(t)$, $T_k^{(m)}(t)$ and $q_{bk}(t)$ are the generalized coordinate of the rail, slab and base at time t ; $Y_{rk}(x)$, $Y_{bk}(x)$ and $X_k^{(m)}(x)$ are the modal functions of the simply supported Euler beam (rail/base) and the free-free Euler beam (slab); NM_r , NM_s and NM_b are the orders of vibration modals of the rail, slab and base; C_{rk} , C_{bk} and D_{sk} are the additional function of gravity which can be calculated by

$$\begin{cases} C_k = \frac{2\sqrt{2ml} \cdot g}{k\pi} (1 - \cos k\pi) \\ \begin{cases} l_s, & \text{for } k = 1 \\ 0, & \text{for } k = 2 \end{cases} \\ D_k = m_s g \times \begin{cases} \frac{\sinh(\beta_k l_s)}{\beta_k} + \frac{\sin(\beta_k l_s)}{\beta_k} \\ -G_k \left[\frac{\cosh(\beta_k l_s)}{\beta_k} - \frac{\cos(\beta_k l_s)}{\beta_k} \right], & \text{for } k > 2 \end{cases} \end{cases} \quad (14)$$

where β_k and G_k are constant coefficients of the free-free beam.

3.2.2 Wheel-rail interaction

The vehicle subsystem and the track subsystem are coupled through the wheel-rail dynamic interaction. In this work, the wheel-rail vertical force is obtained based on the Hertz nonlinear contact theory as follows (Zhai *et al.* 2009)

$$p_j(t) = \begin{cases} \left[\frac{1}{G} \delta Z_j(t) \right]^{3/2}, & \text{for } \delta Z_j(t) > 0 \\ 0, & \text{for } \delta Z_j(t) \leq 0 \end{cases} \quad (15)$$

where G is a constant related to the wheel-rail contact, $\delta Z_j(t)$ is the compression amount at the j th wheel-rail contact point as calculated by

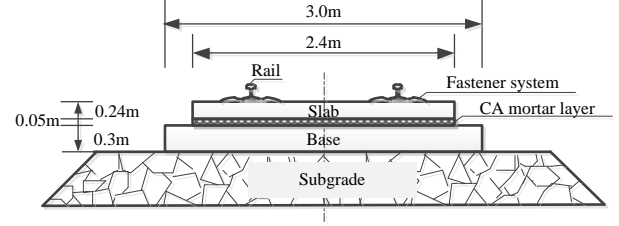


Fig. 7 Cross-section diagram of CRTS I slab track

$$\delta Z_j(t) = Z_{w_j}(t) - Z_r(x_j, t) - Z_{irrej}(t) \quad (16)$$

where $Z_{w_j}(t)$ and $Z_r(x_j, t)$ are respectively the wheel displacement and the rail displacement, $Z_{irrej}(t)$ is the track irregularity as an external excitation.

3.2.3 Numerical integration

The vibration equations of the coupled vehicle-track model can be assembled into an integral matrix equation as

$$\mathbf{M}\ddot{\mathbf{X}} + \mathbf{C}\dot{\mathbf{X}} + \mathbf{K}\mathbf{X} = \mathbf{P} \quad (17)$$

where \mathbf{M} , \mathbf{C} and \mathbf{K} are the mass, stiffness and damping matrices consisting both vehicle and track subsystem; \mathbf{X} , $\dot{\mathbf{X}}$ and $\ddot{\mathbf{X}}$ are the displacement, velocity and acceleration vectors; \mathbf{P} is the generalized force vector of the system.

The large-scale nonlinear system has therefore to be integrated simultaneously in the time domain. This is done by utilizing the simple fast explicit integration method presented by Zhai (1996), which has been proved to be accurate and efficient in solving the second order nonlinear differential equation. The integration algorithm is expressed as

$$\begin{cases} \mathbf{X}_{n+1} = \mathbf{X}_n + \dot{\mathbf{X}}_n \Delta t + (1/2 + \psi) \ddot{\mathbf{X}}_n \Delta t^2 - \psi \ddot{\mathbf{X}}_{n-1} \Delta t^2 \\ \dot{\mathbf{X}}_{n+1} = \dot{\mathbf{X}}_n + (1 + \phi) \ddot{\mathbf{X}}_n \Delta t - \phi \ddot{\mathbf{X}}_{n-1} \Delta t \end{cases} \quad (18)$$

where Δt is the time step, ψ and ϕ are free parameters that control the stability and numerical dissipation of the algorithm, which can be assigned as a value of 0.5 to achieve a good compatibility between numerical stability and accuracy. The subscript n represents the current time step of the integration.

The static responses of the track obtained from Section 3.1 are introduced into the dynamic analysis as the initial condition of the integration. The initial track deflections should be transformed into modal coordinates firstly. The initial velocity of the system is set as zero, and the integration process will be started automatically if let $\phi = \psi = 0$ at the first step. The stable and convergent time step 1×10^{-4} s is assigned to Δt in the present investigation.

4. Demonstration example

4.1 Calculation parameters

In China, it is a common pattern to operate the 300-350 km/h electric multiple unit (EMUs) on non-ballasted tracks (Zhai *et al.* 2015). The typical CRH3 EMU with a running

Table 1 Main parameters of CRH3 high-speed vehicle used in the calculation

Item	Value	Units
Operation speed (v)	300	km/h
Car body mass (M_c)	3.96×10^3	kg
Bogie frame mass (M_b)	3.2×10^3	kg
Wheelset mass (M_w)	2×10^3	kg
Inertia moment of car body about Y axis (J_c)	1.9404×10^6	kg·m ²
Inertia moment of bogie frame about Y axis (J_b)	1.752×10^3	kg·m ²
Primary suspension vertical stiffness (K_{pz})	1.176×10^6	N/m
Primary suspension vertical damping coefficient (C_{pz})	1.96×10^5	N·s/m
Secondary suspension vertical stiffness (K_{sz})	6×10^5	N/m
Secondary suspension vertical damping coefficient (C_{sz})	1.96×10^4	N·s/m
Distance between bogie centres	17.5	m
Bogie wheelbase	2.5	m
Wheel rolling circle radius	0.43	m

Table 2 Main parameters of track-bed used in the calculation

Item	Value	Units
Rail mass per unit length	60.64	kg/m
Rail elastic modulus	2.059×10^{11}	Pa
Area moment of rail cross section	3.217×10^{-5}	m ⁴
Fastener spacing	0.625	m
Vertical stiffness of rail pad	3×10^7	N/m
Vertical damping coefficient of rail pad	2.5×10^4	N·s/m
Elastic modulus of track slab	3.6×10^{10}	Pa
Length of track slab	4.95	m
Density of track slab	2500	kg/m ³
Elastic modulus of concrete base	3.25×10^{10}	Pa
Density of concrete base	2500	kg/m ³
Elastic modulus of CA mortar layer	3×10^8	Pa
Vertical stiffness of subgrade	1.9×10^8	Pa/m
Vertical damping coefficient of subgrade	1×10^5	N·s/m

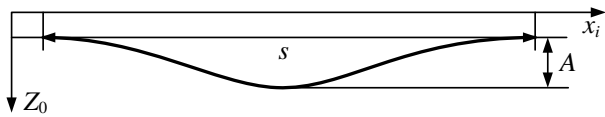


Fig. 8 Differential subgrade settlement described by cosine curve

speed of 300 km/h is adopted in the simulation. The typical unit slab track of China Railway Track System I (CRTS-I) is employed in the present analysis, and the cross-section diagram is shown in Fig. 7. The main parameters of the vehicle and the slab track used in the analysis are listed in Tables 1-2.

The test made by Zhou *et al.* (2011) indicates that the cosine curve (Fig. 8) can be used to describe the profile of differential subgrade settlement. In the settlement section, the subgrade displacement $Z_0(x)$ is defined in Eq. (19).

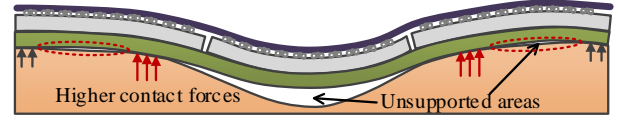


Fig. 9 Schematic diagram of the degraded track due to track self-weight with the differential subgrade settlement of 10 mm/10 m

During the simulation, the settlement amplitude A and settlement wavelength s are set as 10 mm and 10 m, respectively.

$$Z_0(x) = \frac{A}{2} \left(1 - \cos\left(\frac{2\pi x}{s}\right) \right) \quad (19)$$

Additionally, the random track irregularity is inevitable in reality. The average PSD (power spectrum density) of non-ballasted track irregularities of Chinese high-speed railway is employed in this work as an external excitation on the wheel-rail interface (Zeng *et al.* 2015, Zhai *et al.* 2015). The average spectrum of track irregularity can be obtained by piecewise fitting with a power function, which is expressed as

$$S(f) = \frac{A}{f^n} \quad (20)$$

where the unit of $S(f)$ is mm²/(1/m); f is spatial frequency (1/m); A and n are fitting coefficients.

4.2 Static track deflections and interlaminar forces

Primarily, track deflections and unsupported areas due to track weight when there exists subgrade settlement are investigated by means of the semi-analytical method presented in Section 3.1. It permits to detect the initial track state, which further exerts impact on the dynamic behavior of the coupled system. Fig. 9 depicts the schematic diagram of the degraded track subjected to differential subgrade settlement, and how the differential subgrade settlement affects the track level and the interlaminar forces are illustrated in Figs. 10 and 11.

It is visible in Fig. 10 that the slab track settles down to an equilibrium position in the wake of subgrade settlement before the presence of vehicle passage. The deflections of the slabs and the base are almost consistent and apparently different from the subgrade deformation, while the rail deflection differs somewhat from the concrete layers. The reason lies in the high bending stiffness of the track structure, which prevents the track to adjust completely to the situation of the subgrade settlement profile, and the difference in rigidity between the rail and the concrete infrastructure. Local separations of the concrete base from the soil subgrade occur both inside and outside the settlement section. The track structures where are not well supported by the subgrade, namely the unsupported areas are filled with blue in Fig. 10. For the differential subgrade settlement of 10 mm/10 m, the deflection amplitudes of the rail, the slab and the base at settlement centre are only 4.59 mm, 4.60 mm and 4.60 mm respectively. The range of the

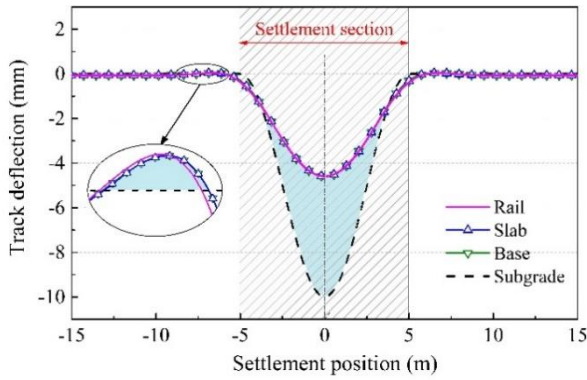


Fig. 10 Track deflections due to track self-weight with the differential subgrade settlement of 10 mm/10 m

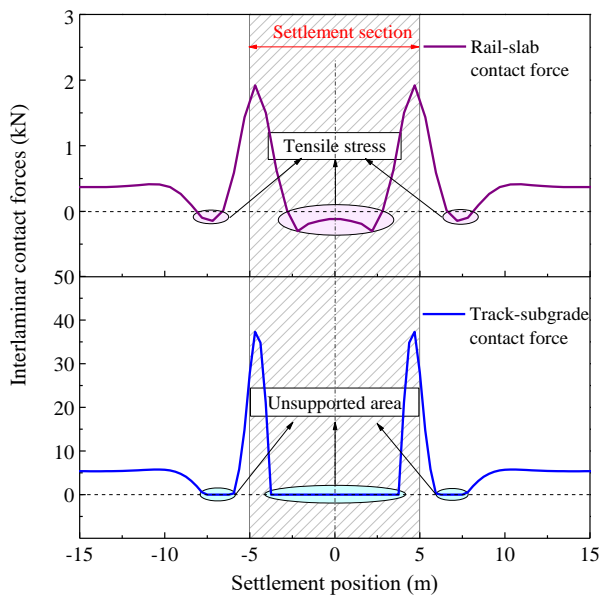


Fig. 11 Rail-slab contact force and track-subgrade contact force due to track self-weight with the differential subgrade settlement of 10 mm/10 m

unsupported area inside the settlement section almost reaches 7.5 m, and the maximum void between the track and the subgrade has a height as large as 5.4 mm. At both sides of the settlement section, the track structure is slightly arched, resulting in two unsupported areas with small gaps approximately 0.05 mm depth between track and subgrade. On this account, the range of the track deflections along the longitudinal direction turns out to show a diffusion with respect to the settlement wavelength.

Uncoordinated deflections of different track layers yield additional stresses on track structure. Fig. 11 shows the rail-slab contact force and the track-subgrade contact force reflected respectively by the resistances of the fastener springs and the subgrade springs aligned along the track. It is clear that the differential subgrade settlement has substantial influences on the distributions of the interlaminar forces. In places distant from the settlement section, the rail-slab contact force and the track-subgrade contact force remain at 5.37 kN and 0.38 kN only subjected to track self-weight. While in the settlement-affected

region, drastic fluctuation arises. For both track-subgrade contact force and rail-slab contact force, two peaks appear near the settlement boundaries at about ± 4.69 m with the maximum values of 37.29 kN and 1.92 kN respectively, indicating that the differential settlement may arouse stress concentrations in particular positions. The results suggest that the positions undergo higher loads are not those ones where are hanging, but generally the places located near the boundary of the settlement section. Those positions bear most of the weight of the adjacent track frame. Three 'zero zones' are occurring on the curve of the subgrade resistance, corresponding to the unsupported areas, where the track is not in complete contact with the subgrade. These three areas correspond to the blue-filled areas in Fig. 10 both at the centre zone of the settlement section and the areas where the track structure is arched. The values of the fastener resistances in these areas are negative, indicating that there are tensile forces between rail and slab. Note that the concrete structure cannot bear large tensile stress, so the settlement-induced structural stresses exerted on the track will inevitably accelerate the deterioration of track components (Sadeghi and Nouban 2017), and the stress concentrations may in turn aggravate the differential settlement of the soil subgrade.

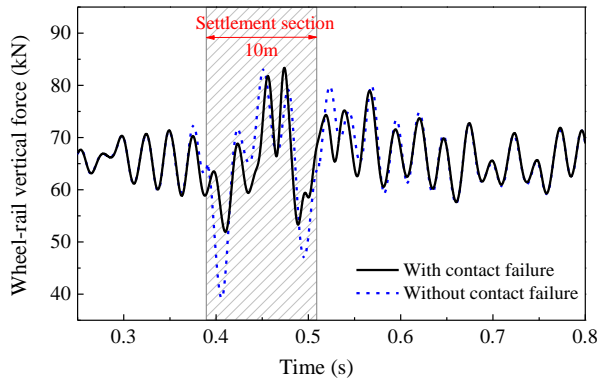
In Fig. 11, contact forces of track-subgrade show higher values than those of rail-slab. The reason is mainly because that the influence of differential subgrade settlement has been attenuated as it propagated through the track structure from bottom to top. The uncoordinated deformations between track and subgrade, as well as the unevenly distributed subgrade stiffness result in dramatic change of track-subgrade contact force. On the other hand, the stiffness of subgrade is times of that of rail pad, which also leads to higher values of the track-subgrade contact force with respect to the rail-slab interaction.

4.3 Dynamic responses of vehicle-track coupled system

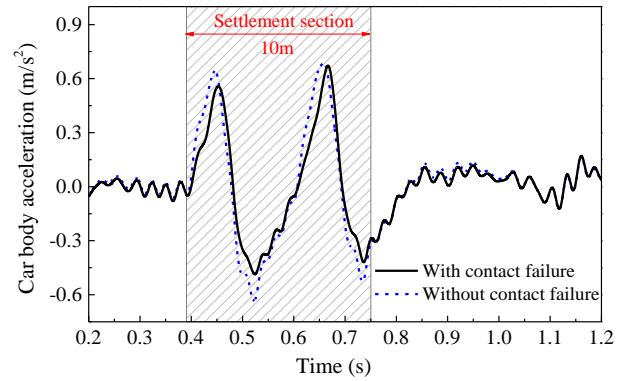
4.3.1 Dynamic responses of vehicle moving on degraded track

Based on the initial track state acquired above, dynamic analysis of the coupled system is performed by loading the high-speed vehicle on the degraded track with a speed of 300 km/h. As mentioned before, in previous studies, perfect contact between track and subgrade is commonly assumed for analysis and design purposes, where the vehicle-track model treats the differential subgrade settlement just as a certain type of track irregularity in accordance with the subgrade deformation. Here, a comparison on dynamic vehicle behaviors calculated between taking or not taking account of the contact failure between the track and the subgrade is illustrated in Fig. 12, in terms of the wheel-rail vertical force and the vertical car body acceleration.

Fig. 12(a) reveals the unloading-loading-unloading process of the leading wheelset as it passes over the settlement section. As seen from the results, the wheel-rail vertical force is susceptible to the degradation of track level. Results of the two simulations are basically in good agreement expect for some small differences occurring inside the settlement section. The wheel-rail force shows an



(a) Wheel-rail vertical force



(b) Car body acceleration

Fig. 12 Comparison of vehicle responses affected by the 10 mm/10 m differential subgrade settlement between simulations with and without consideration of contact failure between track and subgrade

abrupt drop when the wheelset just enters and leaves the settlement section at the time of 0.4 s and 0.5 s, when the wheel unloading rate reaches the maximum. A 25.96 kN drop of the wheel-rail force appears on the result of not considering contact failure between track and subgrade (i.e., “perfect contact”), while it is only 11.60 kN when those unsupported areas are included. The reason why the force variation here of the “perfect contact” situation is much larger lies in the modelling of the settlement boundary. In this simulation, the differential settlement turns out to be exerted directly on the rail. The rail geometry at the settlement boundaries is suddenly changed. Whereas, the transmission and diffusion of the settlement in track structures from down to top are adequately considered in the simulation with contact failure, the track near the settlement boundary is arched and forms a gentle buffer on the rail as the partially enlarged detail in Fig. 10. At the settlement centre, the wheel-rail force is stimulated to a large extent. The peak value of the contact failure situation is 83.36 kN, while that of the “perfect contact” situation is a little lower, 83.17 kN, with a slight offset of the peak position. It is mainly due to the concern of the non-uniform subgrade support. The large-scale unsupported area in the settlement centre between track and subgrade has an effect on the wheel-rail interaction. It also can be found that there is overlapping effect ascribed to subsequent wheelsets. The wheel-rail force continues to fluctuate for a while after the first wheelset moving out of the settlement section. The fluctuation of the “perfect contact” result is severer in the first few time steps out of the settlement section, and then the two results keep consistent.

With respect to the car body acceleration, which is closely associated with the ride comfort of the high-speed train, the vibration is quite severe when the vehicle passes through the differential settlement section compared to the non-settlement section as shown in Fig. 12(b). Two cycles of sinusoidal wave occur as the two bogies successively moves through the settlement section. The maximum accelerations of the two simulations are 0.69 m/s^2 and 0.67 m/s^2 respectively. Due to the damping effect, the oscillation of acceleration attenuates after the vehicle leaves the settlement section, and finally levels off. Within the settlement section, the calculated acceleration of the

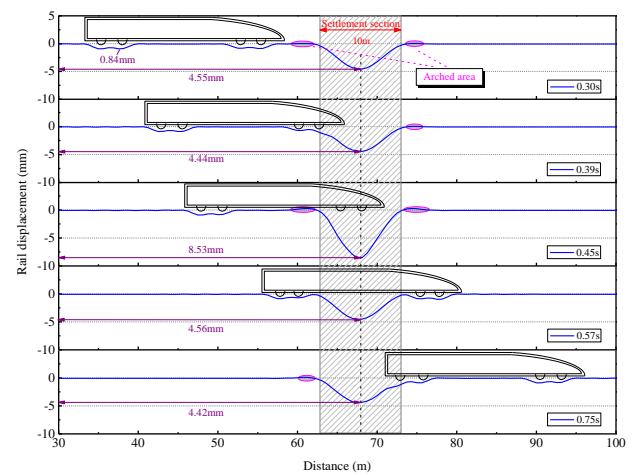


Fig. 13 Variation of dynamic rail displacement during vehicle passing by the 10 mm/10 m differential settlement section

situation considering contact failure between track and subgrade is a little lower than the “perfect contact” situation.

4.3.2 Dynamic responses of track subjected to moving vehicle

The dynamic behaviors of the track subsystem are illustrated in this section. Fig. 13 shows the variation of dynamic rail displacement during the vehicle running through the settlement section. At 0.30 s, before the vehicle arrives at the settlement section, the instantaneous rail displacement under the wheelsets is about 0.84 mm. The amplitude of the settlement-induced rail deflection is 4.55 mm. There are two settlement-induced arched areas on the rail. One of them is compressed at 0.39 s by the rolling wheelset. The rail deflection at the settlement centre is also slightly alleviated to 4.44 mm at that time. When the first wheelset reaches the settlement centre at 0.45 s, the amplitude of rail deflection shows a sudden increase to 8.53 mm due to the combined effect of the vehicle load and the subgrade settlement, and the compressed arched area on the rail reappears. At the time of 0.57 s, the two arched areas suffering the impact of the vehicle from the vehicle are

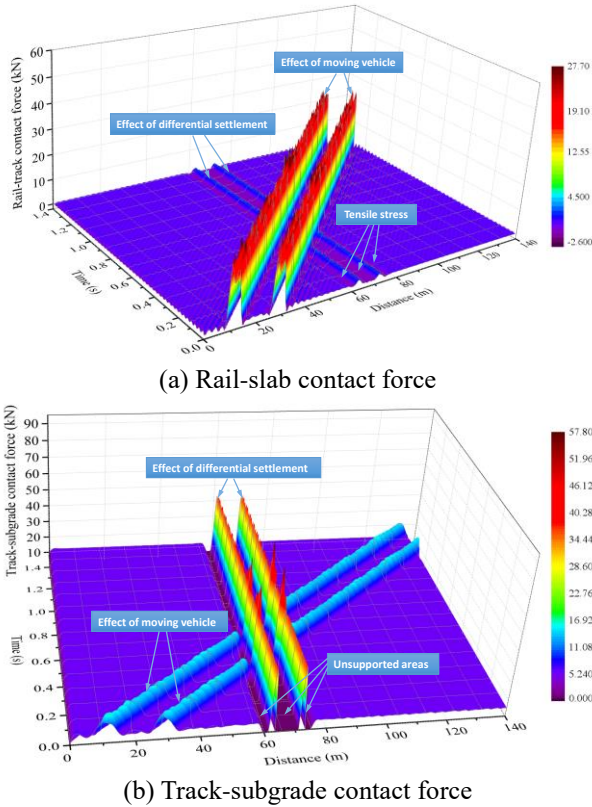


Fig. 14 Variations of interlaminar forces during vehicle passing by the 10 mm/10 m differential settlement section

pressed down. After 0.75 s, when the last wheelset moves out of the settlement section, the amplitude of the rail deflection returns to 4.42 mm, and there is a recurrence of the arched rail. The entire process indicates that the differential settlement plays a dominant role in the rail deflection. The transient impact of the dynamic vehicle load tends to cause abnormal responses of the track vibration, particularly the acute aggravation of the rail displacement at the settlement centre over an unsupported area, as well as the periodical slapping exerted on the arched areas caused by the moving wheelsets. These may not only impair the structural stability, but also impose a risk to the long-term behavior of the whole system.

Fig. 14 illustrates the dynamic rail-slab contact force (i.e., fastener resistance) and the nonlinear subgrade resistance affected by the differential settlement during vehicle passage. In Fig. 14(a), four peaks corresponding to the four wheelsets of the vehicle move over time, and two stationary wave crests locate in the settlement section between 65 m to 75 m which are ascribed to the differential settlement. It is obvious that the vehicle-induced rail-slab force is approximately 22 kN, which is much larger than the maximum value caused by the differential settlement of only 2 kN. From 0.39 s to 0.75 s, as the vehicle passes across the settlement section, the rail-slab force is slightly affected by the overlap of the dynamic load and the differential settlement. When the wheelset moves right over the settlement-induced wave crest, the force can be stimulated up to 27.70 kN. However, when the wheelset reaches the positions where the fasteners are initially in

tension (the arched areas of the track.), the rail-slab contact force under the wheelset will be partly offset and drop to about 18 kN. This indicates that the stress states of the fasteners and adjacent track layers are dynamically changed in coincidence with the appearance and disappearance of the arched track due to vehicle passage, which may exert influence on the fatigue life of the track components.

As shown in Fig. 14(b), different from the rail-slab contact force showed above, the track-subgrade contact force bears the brunt of the differential settlement and somewhat disturbed by the moving vehicle. This is because the track-subgrade contact force at the interface is directly affected by the differential subgrade settlement, while the wheel-rail vertical force attenuates to a large extent as it propagates down through the track structure to the subgrade. Before the vehicle moves into the settlement section, the wheelset-induced track-subgrade contact force is about 15.77 kN, and the maximum value caused by the settlement is 37.53 kN. Three unsupported areas along the track corresponding to those two arched areas near the settlement boundaries and the hanging area around the settlement centre are reflected by the purple-colored areas in the figure, where the track-subgrade contact forces are zero. During the passages of the four wheelsets, the variations of the forces in these three areas show different tendencies. The contacts between the track and the subgrade in the arched areas are lost and re-established periodically, resulting in non-zero values of the track-subgrade force. However, the large-scale hanging area around the settlement centre is always hanging without support from subgrade, even when the wheelset is located on. The only change is that the range of this 'zero area' gets shorter subjected to the dynamic load. Besides, when the wheelset moves over the settlement boundaries where the stress concentrations occur as shown in Fig. 11, the track-subgrade contact force is significantly amplified. The maximum value reaches 57.74 kN subjected to the superposition of the dynamic vehicle impact and the stationary settlement effect.

5. Conclusions

The non-ballasted track is particularly susceptible to the deterioration of the infrastructure due to its strong rigidity and limited adjustability. This paper presents a model to investigate the mechanical behaviors of the coupled vehicle-slab track system affected by differential subgrade settlement that takes into account the track self-weight and the nonlinear subgrade support. The model is applied on the CRTS I non-ballasted slab track which is coupled with a typical high-speed vehicle in China. Both static and dynamic analyses of the system with differential settlement are carried out. Accordingly, the following conclusions can be drawn.

- Differential subgrade settlement greatly accelerates the deterioration of track geometry. The settlement-induced track irregularity exerts drastic impacts on the wheel-rail interaction, and eventually on the running safety and ride comfort of the high-speed train.
- Locally, unsupported areas underneath the track

structure are prone to occurrence due to the non-uniform subgrade support. During dynamic vehicle load, these areas are periodically slapped and the contact between the track and the subgrade here may be lost and/or re-established frequently. The vehicle-track coupled system therefore shows abnormal dynamic behaviors. These will not only impose risks to the operation safety, but also speed up the track deterioration process and impair the long-term service life of the entire system.

- Differential settlement also results in unevenly distributed interlaminar contact forces on track–subgrade structures and disturbed by dynamic load to different extent, particularly the tension stress that is extremely harmful to the concrete structure, and the stress concentrations on the soil subgrade that may promote further settlement.

The application of the proposed model still requires the long-term measured data of the differential subgrade settlement in operating high-speed railways and needs further verification versus field measurements. Nevertheless, it is a general tool for evaluating effect of any possible shape of the settlement profile on the vehicle–track structural stability and systematic dynamics. It is also available for planning of track maintenance and optimizing of track components allowing for the subgrade settlement. Additionally, it can be extended to further prediction of the track settlement evolution.

Acknowledgments

The research described in this paper was supported by the National Basic Research Program of China (“973” Program) (Grant Nos. 2013CB036206, 2013CB036205), the National Natural Science Foundation of China (NSFC) (Grant No. 51678507), and the Program of Introducing Talents of Discipline to Universities (111 Project) (Grant No. B16041).

References

Chen, R., Chen, J., Zhao, X., Bian, X. and Chen, Y. (2014), “Cumulative settlement of track subgrade in high-speed railway under varying water levels”, *Int. J. Rail Trans.*, **2**(4), 205-220.

Chen, Z., Zhai, W., Cai, C. and Sun, Y. (2015), “Safety threshold of high-speed railway pier settlement based on train-track-bridge dynamic interaction”, *Sci. Chin. Technol. Sc.*, **58**(2), 202-210.

Dahlberg, T. (2003), *Railway Track Settlements-A Literature Review*, Report for the EU Project SUPERTRACK, Division of Solid Mechanics, IKP, Linköping University, Linköping, Sweden.

Han, Y.T. and Yao, L. (2007), “Analysis of the dynamic performance for slab track settlement on embankment”, *J. Railw. Eng. Soc.*, **10**, 28-31.

Kouroussis, G., Connolly, D.P., Alexandrou, G. and Vogiatzis, K. (2015a), “The effect of railway local irregularities on ground vibration”, *Transp. Res. D-Tr E*, **39**, 17-30.

Kouroussis, G., Connolly, D.P., Alexandrou, G. and Vogiatzis, K. (2015b), “Railway ground vibrations induced by wheel and rail singular defects”, *Vehic. Syst. Dyn.*, **53**(10), 1500-1519.

Li, G.H., Xu, Z.L., Sun, S.L. and Jing, Z.D. (2007), “The influence of surface subsidence on construction of high-speed railway in

north China plain and its countermeasures”, *J. Railw. Eng. Soc.*, **24**(8), 7-12.

Li, X., Nielsen, J.C. and Pålsson, B.A. (2014), “Simulation of track settlement in railway turnouts”, *Vehic. Syst. Dyn.*, **52**(sup1), 421-439.

Olivier, B., Connolly, D.P., Costa, P.A. and Kouroussis, G. (2016), “The effect of embankment on high speed rail ground vibrations”, *Int. J. Rail Transp.*, **4**(4), 229-246.

Paixão, A., Fortunato, E. and Calçada, R. (2015), “The effect of differential settlements on the dynamic response of the train-track system: A numerical study”, *Eng. Struct.*, **88**, 216-224.

Sadeghi, K. and Nouban, F. (2017), “Behavior modeling and damage quantification of confined concrete under cyclic loading”, *Struct. Eng. Mech.*, **61**(5), 625-635.

Shabana, A.A. and Sany, J.R. (2001), “Asurvey of rail vehicle track simulations and flexible multibody dynamics”, *Nonlin. Dyn.*, **26**(2), 179-210.

Varandas, J.N., Hölscher, P. and Silva, M.A. (2011), “Dynamic behaviour of railway tracks on transition zones”, *Comput. Struct.*, **89**(13), 1468-1479.

Varandas, J.N., Hölscher, P. and Silva, M.A. (2014), “Settlement of ballasted track under traffic loading: Application to transition zones”, *Proc. IMechE, Part F: J. Rail Rap. Trans.*, **228**(3), 242-259.

Wang, B.L., Yang, X.W., Zhou, Y. and Gong, Q.M. (2015), *Subgrade and Track Engineering of High Speed Railway*, 1st Edition, Tongji University Press, Shanghai, China.

Xu, Q.Y., Li, B. and Fan, H. (2012), “Influence of differential settlement of subgrade on dynamic characteristic of train-ballastless track on subgrade coupling system”, *J. Railw. Sci. Eng.*, **9**(3), 13-19.

Zeng, J.C., Zhang, J.W., Tong, X.D. and Tu, Y.M. (2009), “Test evaluation of post-construction settlement of subgrade in Beijing-Shanghai high-speed railway”, *Proceedings of the International Conference on Transportation Engineering*, Chengdu, China, July.

Zeng, Z.P., He, X.F., Zhao, Y.G. and Yu, Z.W. (2015), “Random vibration analysis of train-slab track-bridge coupling system under earthquakes”, *Struct. Eng. Mech.*, **54**(5), 1017-1044.

Zhai, W.M. (1996), “Two simple fast integration methods for large-scale dynamic problems in engineering”, *Int. J. Numer. Meth. Eng.*, **39**(24), 4199-4214.

Zhai, W.M. (2015), *Vehicle-Track Coupled Dynamics*, 4th Edition, Science Press, Beijing, China.

Zhai, W., Liu, P. and Lin, J. (2015), “Experimental investigation on vibration behaviour of a CRH train at speed of 350 km/h”, *Int. J. Rail Trans.*, **3**(1), 1-16.

Zhai, W., Wang, K. and Cai, C. (2009), “Fundamentals of vehicle-track coupled dynamics”, *Vehic. Syst. Dyn.*, **47**(11), 1349-1376.

Zhang, X.H., Burrow, M. and Zhou, S.H. (2016), “An investigation of subgrade differential settlement on the dynamic response of the vehicle-track system”, *Proc. IMechE, Part F: J. Rail Rap. Transit*, **230**(7), 1760-1773.

Zhu, J.J., Ahmed, A.K.W., Rakheja, S. and Khajepour, A. (2010), “Development of a vehicle-track model assembly and numerical method for simulation of wheel-rail dynamic interaction due to unsupported sleepers”, *Vehic. Syst. Dyn.*, **48**(12), 1535-1552.

Zou, C.H., Zhou, S.H. and Wang, B.L. (2011), “Model test study of influence of differential subgrade settlement on ballasted track settlement”, *J. Tongji Univ.*, **39**(6), 862-869.